Acta Pharmaceutica Sinica B 2025;15(5):2480−2497

Chinese Pharmaceutical Association
Institute of Materia Medica, Chinese Academy of Medical Sciences

Acta Pharmaceutica Sinica B

www.elsevier.com/locate/apsb
www.sciencedirect.com

ORIGINAL ARTICLE

Inhibition of CCT5-mediated asparagine biosynthesis and anti-PD-L1 produce synergistic antitumor effects in colorectal cancer

Yujie Zhang[a,b,c,†], Weiyi Zhao[a,d,†], Ling Wu[a,b,c,†], Tianjing Ai[b], Jie He[b], Zetao Chen[e], Chuangyuan Wang[e], Hui Wang[f], Rui Zhou[b], Chaoqun Liu[a], Liang Zhao[a,b,c,*]

[a]*Department of Pathology, Nanfang Hospital, Southern Medical University Guangzhou 510515, China*
[b]*Department of Pathology & Guangdong Province Key Laboratory of Molecular Tumor Pathology, School of Basic Medical Sciences, Southern Medical University, Guangzhou 510515, China*
[c]*Department of Pathology, Shunde Hospital, Southern Medical University (the First People's Hospital of Shunde), Foshan 528399, China*
[d]*Department of Pathology, the Second Affiliated Hospital, Zhejiang University School of Medicine, Zhejiang University, Hangzhou 310009, China*
[e]*Department of Neurosurgery, Zhujiang Hospital, Southern Medical University, Guangzhou 510260, China*
[f]*Department of Medical Oncology, Affiliated Tumour Hospital of Guangzhou Medical University, Guangzhou 510095, China*

Received 15 December 2024; received in revised form 16 February 2025; accepted 18 February 2025

KEY WORDS

Colorectal cancer;
CCT5;
Asparagine metabolism;
ASNase;
Anti-PD-L1 immunotherapy;
Combination therapy;
$CD8^+$ T cell;
ASNS

Abstract Abnormal amino acid metabolism promotes tumor progression by inducing malignant behaviors in tumor cells and altering the immune landscape within the tumor microenvironment. However, the underlying mechanisms remain unclear. In this study, we constructed colorectal cancer (CRC) organoids and patient-derived tumor xenograft (PDX) models, performing multifaceted validation to confirm that T-complex protein 1 subunit epsilon (CCT5), mediates the biosynthesis of aspartate and enhances sensitivity to anti-PD-L1 immunotherapy. Mechanistically, CCT5 directly binds to asparagine synthetase (ASNS) and promotes the synthesis of aspartate (Asn). The Asn−mTORC1 axis facilitates tumor cell proliferation while upregulating PD-L1 expression, which leads to a reduction in the number of effector $CD8^+$ T cells. Treatment with L-asparaginase (ASNase) combined with anti-PD-L1 therapy effectively

*Corresponding author.
E-mail address: liangsmu@foxmail.com (Liang Zhao).
[†]These authors made equal contributions to this work.

Peer review under the responsibility of Chinese Pharmaceutical Association and Institute of Materia Medica, Chinese Academy of Medical Sciences.

https://doi.org/10.1016/j.apsb.2025.03.026

reverses the growth of CRC characterized by high CCT5 expression. In summary, we identify CCT5 as a potential biomarker to guide the combined use of ASNase and anti-PD-L1 antibodies in CRC treatment.

1. Introduction

Colorectal cancer (CRC) ranks third in prevalence and second in mortality among all types of cancer[1]. Over the past decade, the focus of CRC treatment has shifted from systemic radiotherapy and chemotherapy to precise therapies targeting molecular drivers and immunotherapy aimed at the protective tumor microenvironment (TME)[2]. However, due to the high molecular heterogeneity of CRC, many patients do not benefit from advanced clinical treatments. Clinical trials have shown that individualized treatment based on tumor molecular and pathological characteristics can improve overall survival rates[3]. Therefore, in addition to exploring new drugs and therapeutic strategies, it is urgent to develop new molecular biomarkers that can stratify CRC patients for precise treatment based on their unique biological characteristics.

Chaperone proteins were initially identified for their role in folding and preventing protein aggregation under stress conditions. Recent research has revealed their significant association with various aspects of tumorigenesis[4], progression[5], therapy resistance[6], and immune tolerance induction[7] across multiple cancer types. This highlights their potential as diagnostic and prognostic biomarkers, as well as novel therapeutic targets for cancer[8,9]. The T-complex protein 1-ring complex (TRiC, also known as CCT) is a Group II eukaryotic cytosolic chaperonin that consists of two sets of eight subunits (CCT1−8) forming an identical hetero-oligomeric ring[10]. T-complex protein 1 subunit epsilon (CCT5) is one of the subunits of TRiC. According to existing literature, CCT5 can bind to proteins and participate in multiple biological processes such as embryonic development, cell cycle regulation, and cell migration, thereby promoting the metastasis of gastric and lung cancer[11,12].

Specific metabolic activities contribute to biological processes that promote tumor growth[13]. A recent study revealed a significant increase in various amino acid metabolites in both mouse and human CRC, suggesting a role for dysregulated amino acid metabolism[14]. Reprogramming of amino acid metabolism partially fulfills the heightened nutritional demands for tumor proliferation under nutrient-limited conditions[15]. Amino acid deprivation may be an effective strategy for tumor treatment[16]. In recent years, asparagine (Asn) has been implicated in tumor progression[17,18]. Asparagine synthetase (ASNS) catalyzed *de novo* Asn synthesis, which consumes glutamine and ATP, and plays a critical role in protein synthesis. L-asparaginase (ASNase), which deprives Asn by hydrolyzing it to aspartate, has been used as a first-line treatment for childhood acute lymphoblastic leukemia (ALL)[19]. Although ASNase has been reported to exhibit therapeutic effects in solid tumors, including ovarian cancer, pancreatic cancer, breast cancer, and CRC[17,18], the absence of accurate biomarkers significantly limits its clinical application. The personalized therapeutic effect of ASNase in CRC patients remains unclear.

Reprogramming tumor amino acid metabolism not only affects tumor cell survival and proliferation but also impacts the surrounding TME[20,21]. Multiple studies have shown that aberrant amino acid metabolism in tumor cells can promote T cell dysfunction and exhaustion, leading to evasion of immunological surveillance and facilitating tumor progression[22,23]. The therapeutic potential of targeting abnormal amino acid metabolism to enhance anti-tumor immunity has been preliminarily validated in various tumor types, including CRC[22,24,25].

In this study, functioning as a molecular chaperone that regulates the homeostasis of intercellular proteins, CCT5 was first found to be involved in the regulation of Asn metabolism and to mediate $CD8^+$ T cell immunosuppression. Most importantly, we propose CCT5 as a specific biomarker and then support the application of ASNase combined therapy with programmed death-ligand 1 (PD-L1) antibody treatment in patients with CRC with high CCT5 expression.

2. Materials and methods

2.1. Cell lines and cell culture

The NCM460 cell line, derived from normal colon epithelial cells, along with various human colorectal cancer cell lines (SW480, SW620, HCT116, RKO, HCT15, LoVo, and Caco-2) and the human embryonic kidney cell line 293T, were procured from the Cell Bank of Type Culture Collection of the Chinese Academy of Sciences (Shanghai, China). All cell lines were cultured in RPMI 1640 medium (KeyGEN BioTECH, Jiangsu, China) supplemented with 10% fetal bovine serum (FBS, Gibco-BRL, Invitrogen, Paisley, UK). Cells were maintained in a humidified atmosphere containing 5% CO_2 at 37 °C. All cell lines used in this study were negative for mycoplasma and were authenticated by short tandem repeat (STR) profiling within four years.

The final concentrations of the chemicals used for the *in vitro* treatment of CRC cells or CRC patient-derived tumor organoids (PDTOs) in this study are listed as follows: 10 nmol/L rapamycin (RAPA, S1039, Selleckchem, Houston, TX, USA) for CRC cells and 10 μmol/L for PDTOs; 2 UI/mL L-asparaginase (ASNase, ENZ-287, ProSpec, East Brunswick, NJ, USA); 0.1 mmol/L L-asparagine (A8381, Sigma−Aldrich, St. Louis, MO, USA); 4 mmol/L L-albizziine (Alb, A-230-250, Goldbio, MO, USA); and 50 μg/mL anti-PD-L1 antibody (atezolizumab, αPD-L1, A2004, Selleckchem, Houston, TX, USA). Transfection of cells with plasmid vectors and siRNAs was performed using Lipofectamine 3000 reagent (ThermoFisher Scientific, MA, USA), following the guidelines provided by the manufacturer's instructions.

2.2. Clinical tissue samples

Fresh clinical CRC tissues were obtained from the general surgery department at Shunde Hospital, Southern Medical University (Foshan, China) after informed consent was obtained from patients. Formalin-fixed paraffin-embedded tissue samples were

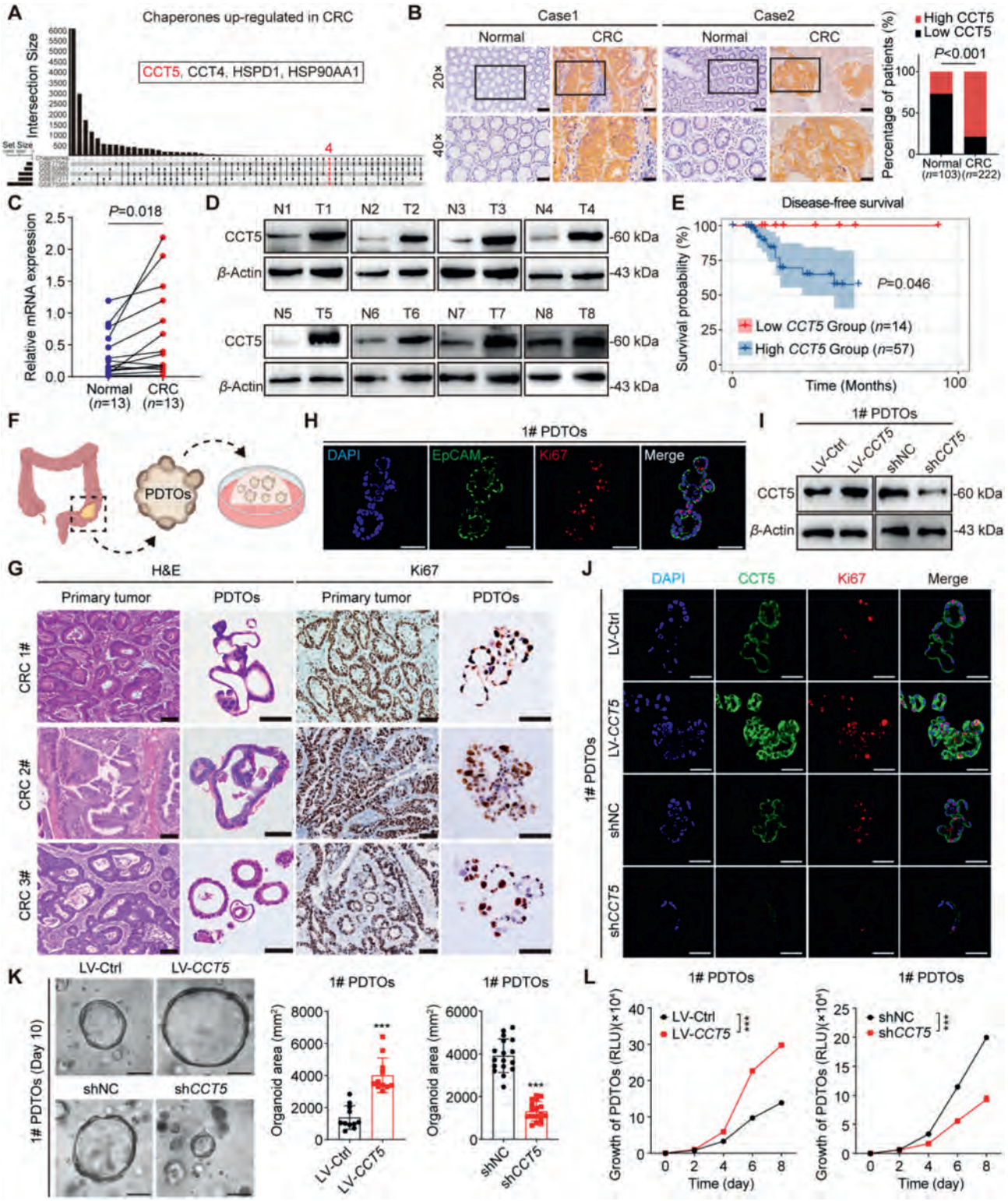

Figure 1 Malignant high expression of CCT5 promotes CRC proliferation. (A) The Upset diagram illustrates the overlap of differentially expressed genes (DEGs) between normal tissues and CRC in the CRC datasets with the chaperone proteins set. (B) Immunohistochemistry (IHC) was performed to detect the expression of CCT5 in CRC tissues and adjacent normal mucosal tissues. Scale bar = 100 μm for the 20× figures and 50 μm for the 40× figures. n = 103 (normal) and 222 (CRC). (C, D) qPCR (n = 13) (C) and Western blot assays (n = 8) (D) demonstrate the expression of CCT5 in fresh CRC tissues (T) and paired normal mucosa (N). (E) The Kaplan−Meier survival curve demonstrates a relationship between CCT5 expression and disease-free survival (DFS) in CRC patients from the Shunde Hospital cohort. n = 14 (low *CCT5*) and 57 (high *CCT5*). (F) A schematic diagram shows the construction of tumor organoids derived from CRC patients. (G) Representative images of H&E and IHC staining for Ki67 in PDTOs and corresponding primary tumors. Scale bar = 100 μm. (H) Representative images of IF staining for EpCAM

collected from 222 cases of primary CRC patients, and the 103 CRC tissues with paired normal mucosa were obtained from the Tumor Tissue Bank of Shunde Hospital, Southern Medical University. The clinical follow-up data for these samples is all available. In each case, a diagnosis of primary CRC had been made before the elective surgery was carried out at Shunde Hospital between 2017 and 2022. None of the patients had received any preoperative chemotherapy or radiotherapy before surgery. The Ethics Committee of Shunde Hospital, Southern Medical University has approved the study (Foshan, China) (Application No: KYLS20230731), and all aspects of the study comply with the Declaration of Helsinki.

2.3. CRC patient-derived tumor organoids culture

PDTOs were constructed as previously described[26]. PDTOs were established using fresh tissue obtained from colon adenocarcinoma patients. Fresh patient tumor tissues were mechanically minced, and digested using Tumor tissue digestion solution (K601003, bioGenous, Hangzhou, China) at 37 °C for 30 min, and filtered through a 100 μm mesh. The filtered samples were then centrifuged at 300×*g* for 5 min (Centrifuge, 5810R, Eppendorf, Hamburg, Germany). The organoids were mixed with Matrigel (356231, Corning, NY, USA), and the mixture was seeded into 24-well plates. The culture medium (K2103-CR, bioGenous, Hangzhou, China) was added after the Matrigel solidified and was refreshed every 2 days. The organoids were passaged every 7−14 days by dissociation with an organoid dissociation solution (E238001, bioGenous, Hangzhou, China).

Gene editing of PDTOs was performed according to previously established protocols[26]. The viral supernatant was concentrated *via* high-speed centrifugation at 80,000×*g* for 2 h at 4 °C (Centrifuge, Optima XPN-100, Beckman, Fullerton, CA, USA). The collected viral particles were resuspended in an organoid culture medium containing 8 μg/mL polybrene (107689, Sigma−Aldrich, St. Louis, MO, USA), followed by a 4 h incubation with the organoids. The organoids were then embedded in Matrigel and incubated in an organoid culture medium supplemented with 10 μmol/L Y-27632 (S6390, Selleckchem, Houston, TX, USA). Approximately 48 h after viral infection, organoids were selected in a culture medium containing 2 μg/mL puromycin (s7417, Selleckchem, Houston, TX, USA) for seven consecutive days. The PDTOs were seeded in 96-well plates and incubated. PDTOs growth was evaluated using the CellTiter-Glo 3D cell viability assay (G9683, Promega, Madison, WI, USA) according to the manufacturer's instructions. Luminescence was quantified using a Synergy Neo2 HTS multimode microplate reader (BioTek, Winooski, VT, USA).

2.4. Animals, subcutaneous tumor models, PDX models, and treatment

The 3−5-week-old male BALB/c mice weighing 15−20 g were purchased from the Nanfang Medical University Experimental Animal Center (Guangzhou, China). All animal experiments were approved by the Institutional Animal Care and Use Committee of Nanfang Hospital, Southern Medical University (Guangzhou, China) (Application No: NFYY-2021-0566). The gene-edited CT26 cells were resuspended in PBS and injected subcutaneously into the flanks of the hind legs on both sides of the mice.

We examined the expression of CCT5 in primary tumor tissues of different patients by WB and classified them into high and low-expression groups. The patient-derived tumor xenograft (PDX) model was established by subcutaneous inoculation of fresh CRC patient tissue fragments into 6-week-old male NSG mice, which were purchased from Guangdong Zhiyuan Biopharmaceutical Technology Co., Ltd. (Guangzhou, China). The specific build information is as previously described[27]. When PDX mice are passed on to the 3rd generation for dosing treatment. Start treatment when tumor volume reaches 100−200 mm^3.

The mice were treated with PBS or ASNase (5 IU/g of body weight, ENZ-287, ProSpec, East Brunswick, NJ, USA) intraperitoneally (i.p.) every 3 days, and isotype IgG (A2116, Selleckchem, Houston, TX, USA) or anti-PD-L1 antibody (10 mg/kg, A2115, Selleckchem, Houston, TX, USA) every 6 days. Tumor size was measured using a Vernier caliper, and tumor volume (mm^3) was calculated according to Eq. (1):

$$\text{Tumor volume} = \text{Length} \times (\text{Width})^2/2 \quad (1)$$

The tumor growth inhibitory value (TGI) was calculated according to Eq. (2)

$$\text{TGI} = (1 - (\text{TV}_{\text{treated Day } n} - \text{TV}_{\text{treated Day 0}}) / (\text{TV}_{\text{control Day } n} - \text{TV}_{\text{control Day 0}})) \times 100\% \quad (2)$$

Here, TV represents the tumor volume, treated represents the drug treatment group, and control represents the control group. *n* represents the final day of treatment and 0 represents the first day of treatment.

After approximately 4−6 weeks, euthanize the mice using carbon dioxide as an anesthetic. Hematoxylin and eosin (H&E) staining of the lungs shows no evidence of pulmonary hemorrhage in the mice (Supporting Information Fig. S1A). H&E staining of the liver, spleen, and kidneys also shows no signs of abnormal tissue damage (Fig. S1B). This complies with animal ethics. The subcutaneous tumor tissue was collected for subsequent histological examination.

2.5. Statistical analyses

Public microarray data were downloaded from The Cancer Genome Atlas (TCGA) datasets (http://cancergenome.nih.gov/) and GEO databases (http://www.ncbi.nlm.nih.gov/geo/). Gene set enrichment analysis (GSEA) was performed using GSEA 4.0.2 software (http://www.broadinstitute.org/gsea/). Figures and graphical elements in this manuscript were created and compiled using BioRender (https://www.biorender.com/) and Adobe Illustrator 2020 (Adobe, San Jose, CA, USA). The results were analyzed using SPSS statistical software

and Ki67 in PDTOs. Scale bar = 50 μm. (I) Western blot verification of the efficiency of 1# PDTOs overexpression and knockdown of *CCT5*. $n = 3$. (J) Representative images of IF staining for CCT5 and Ki67. Scale bar = 50 μm. $n = 3$. (K) Representative images of 1# PDTOs before and after the manipulation of *CCT5* expression. Scale bar = 50 μm. The statistical chart shows the average area of PDTOs under a 40× magnification field of view. $n = 3$. (L) Growth curves of PDTOs after the manipulation of *CCT5* expression. $n = 3$. Data are represented as mean ± SD. $^{***}P < 0.001$.

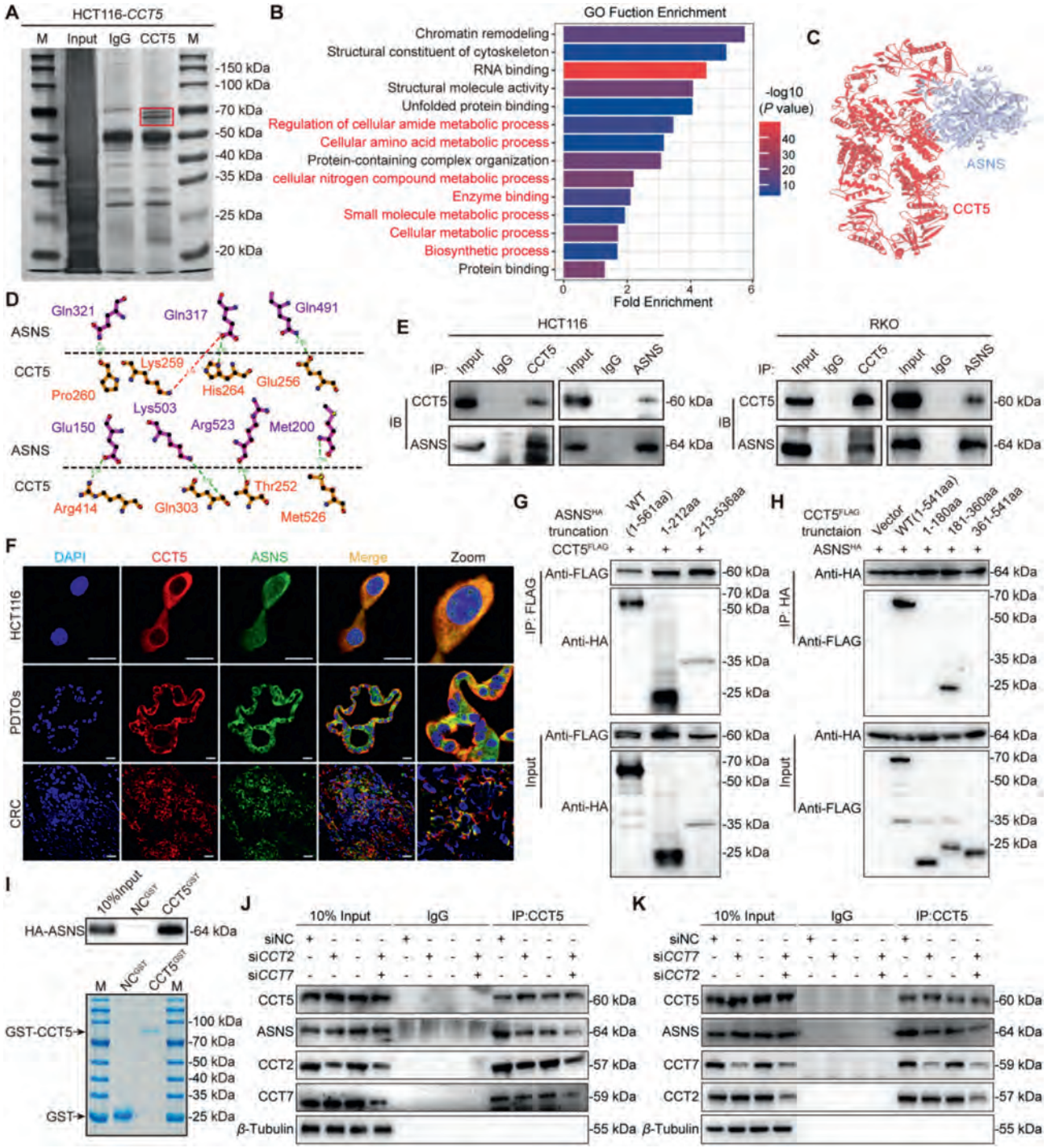

Figure 2 CCT5 interacts with ASNS. (A) The red box enclosed in the silver stain results shows the differential expression bands of CCT5-interacting proteins after IP conducted by the CCT5 antibody. (B) GO functional analysis of CCT5-interacting proteins detected by MS analysis. (C) The molecular docking model of CCT5 and ASNS was performed in HDOCK SERVER (http://hdock.phys.hust.edu.cn/). (D) A simplified version of the 2D interaction diagram of CCT5 and ASNS. See also Supporting Information Fig. S7C. (E) Co-IP assays were conducted to elucidate the intrinsic interaction between CCT5 and ASNS. $n = 3$. (F) Fluorescence colocalization images demonstrate that CCT5 and ASNS are co-localized in HCT116 cells, PDTOs, and CRC tissues. The Scale bar = 20 μm. $n = 3$. (G, H) Western blot results indicate the binding domains of CCT5 and ASNS in 293T cells demonstrated by Co-IP using ASNS (G) or CCT5 (H) truncation variants. $n = 3$. See also Supporting Information Fig. S7E. (I) GST pull-down assay demonstrates the direct binding between CCT5 and ASNS. $n = 3$. (J, K) Co-IP experiments with CCT5 antibody in the presence or absence of *CCT2* (J) or *CCT7* (K) siRNA in 293T cells. $n = 3$.

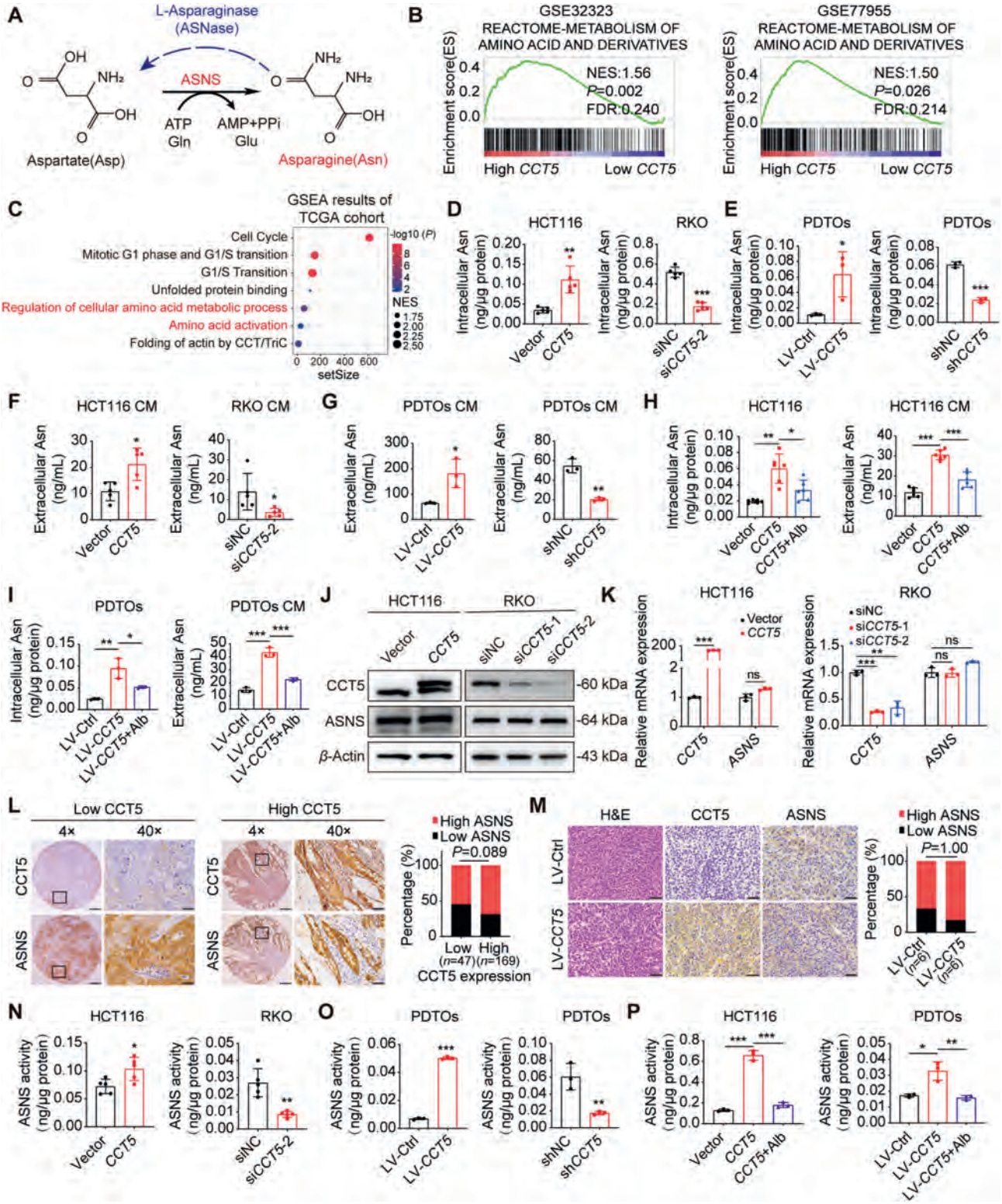

Figure 3 CCT5 interacts with ASNS to increase asparagine biosynthesis. (A) The schematic diagram shows the *de novo* biological synthesis of asparagine. (B) GSEA analysis results from GSE32323 and GSE77955 CRC datasets. (C) GSEA analysis shows the enriched pathways in *CCT5* overexpression CRC samples from the TCGA database. (D, E) LC−MS detects the intracellular Asn level in HCT116 cells ($n = 5$) (D) and PDTOs ($n = 3$) (E). (F, G) LC−MS detects the extracellular Asn level in cell culture medium (CM) in RKO cells ($n = 5$) (F) and PDTOs ($n = 3$) (G). (H, I) The influence of L-albizziine (Alb) on CCT5-mediated Asn synthesis in HCT116 cells ($n = 6$) (H) and PDTOs ($n = 3$) (I). (J, K) Western blot (J) and qPCR assays (K) were performed to verify the expression of ASNS. $n = 3$. (L) IHC analysis shows the relationship between the expression of ASNS and CCT5 in CRC tissues. Scale bar = 500 μm in 4× figures; Scale bar = 50 μm in 40× figures. $n = 47$ (low CCT5) and 169 (high CCT5). (M) The IHC assay shows the relationship between the expression of ASNS and CCT5 in subcutaneous tumors. Scale bar = 50 μm. $n = 3$. (N, O) Asn levels generated by CRC cells ($n = 5$) (N) and PDTOs ($n = 3$) (O) *in vitro* were assayed by LC−MC to reflect ASNS activity (ng/μg protein). (P) The influence of Alb on the CCT5-mediated ASNS activity. $n = 3$. Data are represented as mean ± SD. $^*P < 0.05$; $^{**}P < 0.01$; $^{***}P < 0.001$; ns not significant.

(version 24.0, *SPSS*, Inc., Chicago, IL, USA) and GraphPad Prism 8 software (*GraphPad Software*, Inc., CA, USA). Statistical tests included Student's *t*-tests (paired or unpaired), one-way ANOVA, Pearson Correlations, Pearson's chi-squared test (χ^2), and Kaplan−Meier analysis. $P < 0.05$ was considered statistically significant ($^*P < 0.05$, $^{**}P < 0.01$, $^{***}P < 0.001$, ns not significant).

3. Result

3.1. CCT5 is upregulated in CRC predicts a poor prognosis and promotes the proliferation of PDTOs

Chaperone proteins play a crucial and irreplaceable role in tumor biology. To identify potential molecular chaperone biomarkers in CRC, we analyzed integrated gene expression profiles from five human CRC datasets obtained from the Gene Expression Omnibus (GEO) database (GSE39582, GSE73360, GSE77955, GSE83889, and GSE87211). By cross-referencing the upregulated genes in these datasets with a chaperone protein set, we identified four differentially expressed chaperone proteins: *CCT5*, *CCT4*, *HSPD1*, and *HSP90AA1* (Fig. 1A). Notably, *CCT5* was identified as the sole molecular chaperone associated with poor prognosis in CRC (Supporting Information Fig. S2A). *CCT5* is a subunit of the molecular chaperone TRiC. We further analyzed the effects of other subunits of this complex on the prognosis of CRC. The results indicated that *CCT5* independently contributes to poor prognosis in CRC (Fig. S2B). The expression of *CCT5* was significantly upregulated in CRC tissues compared to normal colorectal mucosa (Supporting Information Fig. S3A and S3B) and in paired CRC tissues (Fig. S3C). Clinical sample analysis revealed that CCT5 is highly expressed in CRC tissues (Fig. 1B−D), and elevated CCT5 expression is positively correlated with poor disease-specific survival in the Shunde Hospital cohort (Fig. 1E). Additionally, we observed higher CCT5 expression in CRC cell lines compared to normal colonic epithelial NCM460 cells (Fig. S3D−S3F). These findings strongly suggest that high CCT5 expression is associated with a poor prognosis in CRC.

To more effectively preserve the heterogeneity of CRC, we established patient-derived tumor organoids (PDTOs) from fresh human CRC samples (Fig. 1F). The three PDTOs showed a high degree of consistency with the original tumor tissues in terms of morphological characteristics and Ki67 expression levels (Fig. 1G). The PDTOs were circular or oval with a hollow lumen, and the expression of EpCAM and Ki67 in the PDTOs indicated their epithelial characteristics and proliferative capacity (Fig. 1H). Subsequently, we performed overexpression and knockdown treatments in CRC 1# PDTOs to manipulate the expression of *CCT5* (Fig. 1I). The Ki67 expression and growth of PDTOs were significantly affected by changes in *CCT5* expression (Fig. 1J−L). We similarly constructed CRC cell lines with *CCT5* overexpression and knockdown (Supporting Information Fig. S4A and S4B, and Supporting Information Fig. S5A). The results showed that CCT5 promoted CRC cell proliferation both *in vivo* and *in vitro* (Figs. S4C−S4E, S5B and S5C). Furthermore, the expression levels of other TRiC complex subunits did not significantly change with alterations in *CCT5* expression, indicating that the changes in CRC proliferation capacity are primarily regulated independently by CCT5 (Supporting Information Fig. S6).

3.2. Direct interaction between CCT5 and ASNS in CRC

To elucidate the potential mechanisms underlying CCT5-mediated CRC proliferation, we conducted an immunoprecipitation (IP) experiment using a CCT5-specific antibody to enrich CCT5-interacting proteins. We identified three distinct bands at positions of 50−70 kDa, which were absent in the IgG control group (Fig. 2A). Subsequent qualitative mass spectrometry (MS) assays and GO function enrichment analysis of the identified proteins revealed significant enrichment in small molecule metabolism, enzyme binding, and biosynthetic processes, suggesting a role for CCT5 in these biological processes in CRC (Fig. 2B). ASNS was identified based on its ranking (Supporting Information Fig. S7A and S7B). Molecular docking results indicated potential binding between ASNS (amino acids 321, 317, 491, 150, 503, 523, and 200) and CCT5 (amino acids 260, 259, 264, 256, 414, 303, 252, and 526) (Fig. 2C and D, Fig. S7C). Our study confirmed the interaction and spatial co-localization between CCT5 and ASNS (Fig. 2E and F). Additionally, truncated plasmids with fusion tags were constructed (Fig. S7D), demonstrating that amino acids 181−360 of CCT5 can bind to both truncated variants of ASNS (Fig. S7E, Fig. 2G and H). GST pull-down experiments further confirmed the direct binding of CCT5 to ASNS (Fig. 2I and Fig. S7F). To determine whether the binding of CCT5 to ASNS is dependent on the integrity of the TRiC complex, we knocked down the adjacent subunits *CCT2* and *CCT7* to disrupt its function[28]. Our results showed that the knockdown of *CCT2* or *CCT7* alone or both simultaneously did not affect CCT5 expression, and CCT5 binding to ASNS was reduced but still present (Fig. 2J and K). This finding suggests that CCT5 can specifically bind to ASNS independently of the integrity of the TRiC complex.

3.3. CCT5 stimulates the activity of ASNS to increase Asn biosynthesis

In biological organisms, aspartate and glutamine serve as substrates for the biosynthesis of Asn catalyzed by ASNS in the presence of ATP. Remarkably, ASNase was capable of reversing this process[29] (Fig. 3A). Pathways related to the regulation of amino acid metabolism and activation were enriched in CRC tissues with high *CCT5* expression (Fig. 3B and C, Supporting Information Fig. S8A). This finding is consistent with the GO enrichment results for CCT5-interacting proteins (Fig. 2B). Liquid chromatography−mass spectrometry (LC−MS) was employed to detect Asn levels. As predicted, *CCT5* expression positively correlated with Asn levels in CRC cells, PDTOs, and the corresponding culture medium (CM) (Fig. 3D−G). L-Albizziine (Alb), a competitive inhibitor of ASNS, reversed the increased Asn levels induced by *CCT5* overexpression (Fig. 3H and I). Additionally, it was observed that changes in *CCT5* expression did not affect ASNS transcription or protein levels (Fig. 3J−M). Surprisingly, CCT5 enhanced ASNS activity to generate more Asn *in vitro* (Fig. 3N and O, Fig. S8B). The increase in Asn levels was reversed after treatment with Alb (Fig. 3P).

3.4. The Asn/mTORC1 axis plays a critical role in CCT5-mediated CRC proliferation

To investigate the mechanism by which CCT5 mediates CRC proliferation *via* Asn, we performed Gene Set Enrichment Analysis (GSEA) on four CRC datasets based on *CCT5* expression profiles and identified their intersection (Fig. 4A). The results indicated that the mTORC1 signaling pathway is significantly and positively associated with high *CCT5* expression (Fig. 4B). It has been demonstrated that Asn can function as an amino acid exchange molecule to activate the mTORC1 signaling pathway in

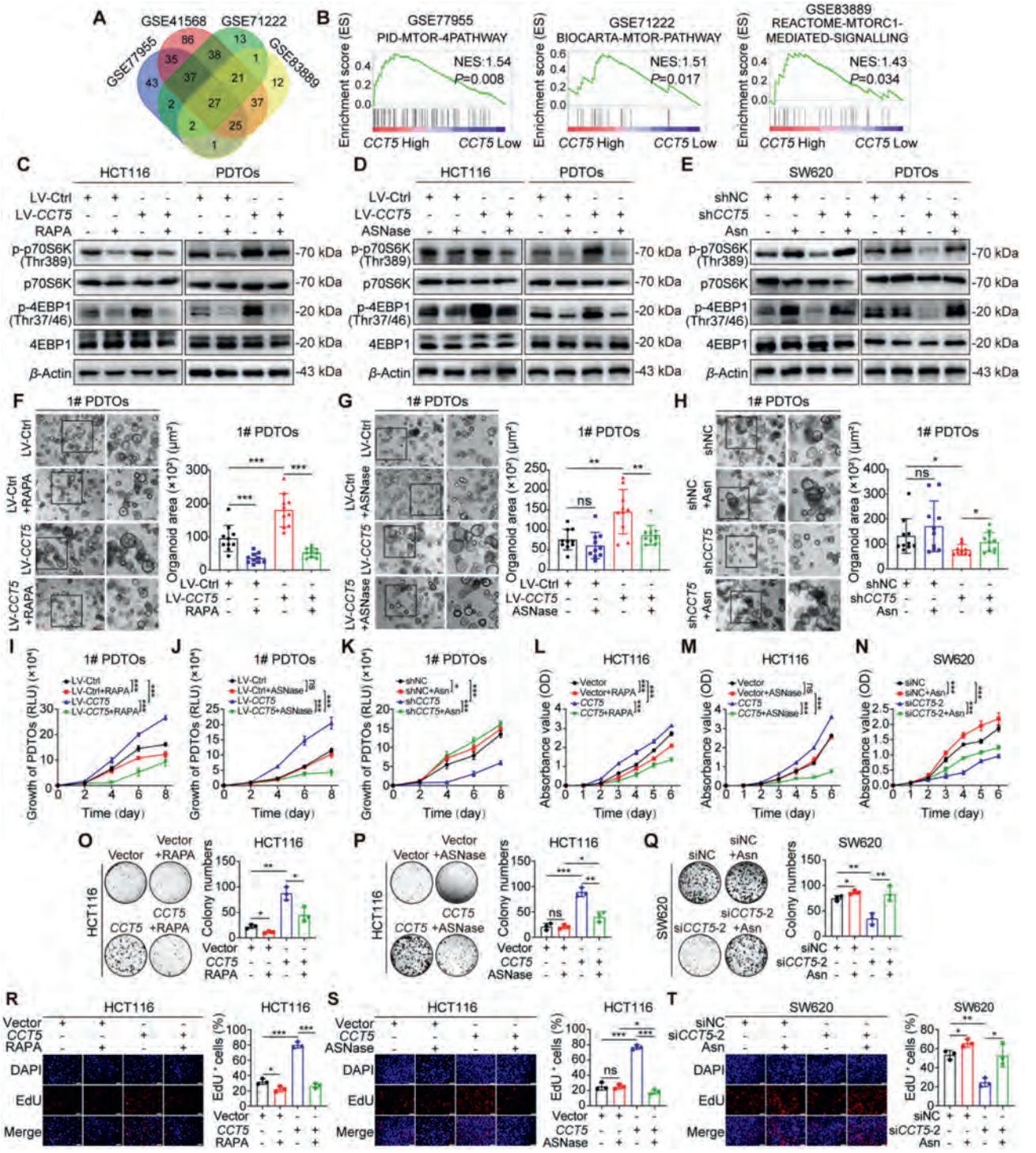

Figure 4 The Asn/mTORC1 axis plays a critical role in CCT5-mediated CRC proliferation. (A) Venn diagram of GSEA results of *CCT5* expression profiles in four CRC datasets. (B) GSEA analysis indicates the enrichment of the mTORC1 signaling pathway in CRC tissues with high *CCT5* expression. (C−E) Western blot assays demonstrate the expression of mTORC1 pathway components in the *CCT5*-manipulated HCT116 cells and PDTOs with or without RAPA (C), ASNase (D), or Asn (E) treatment. $n = 3$. (F−H) Representative light field images of the *CCT5* expression-manipulated PDTOs treated with or without RAPA (F), ASNase (G), or Asn (H). The Scale bar = 100 μm. The statistical chart shows the average area of PDTOs under a 40× magnification field of view. $n = 3$. (I−K) Growth curves of the *CCT5*-manipulated PDTOs cultured in a medium with or without the treatment of RAPA (I), ASNase (J), or Asn (K). $n = 3$. (L−N) CCK-8 analysis shows the effects of RAPA (L), ASNase (M), or Asn (N) on the proliferation of *CCT5* expression manipulated CRC cells. $n = 3$. (O−Q) Colony formation assays indicate the effect of RAPA (O), ASNase (P), or Asn (Q) on the proliferation of *CCT5*-manipulated CRC cells. $n = 3$. (R−T) *EdU* incorporation assays investigate the effects of RAPA (R), ASNase (S), or Asn (T) on the proliferation of *CCT5* expression-manipulated CRC cells. The scale bar = 100 μm. $n = 3$. Data are represented as mean ± SD. $^*P < 0.05$; $^{**}P < 0.01$; $^{***}P < 0.001$; ns not significant.

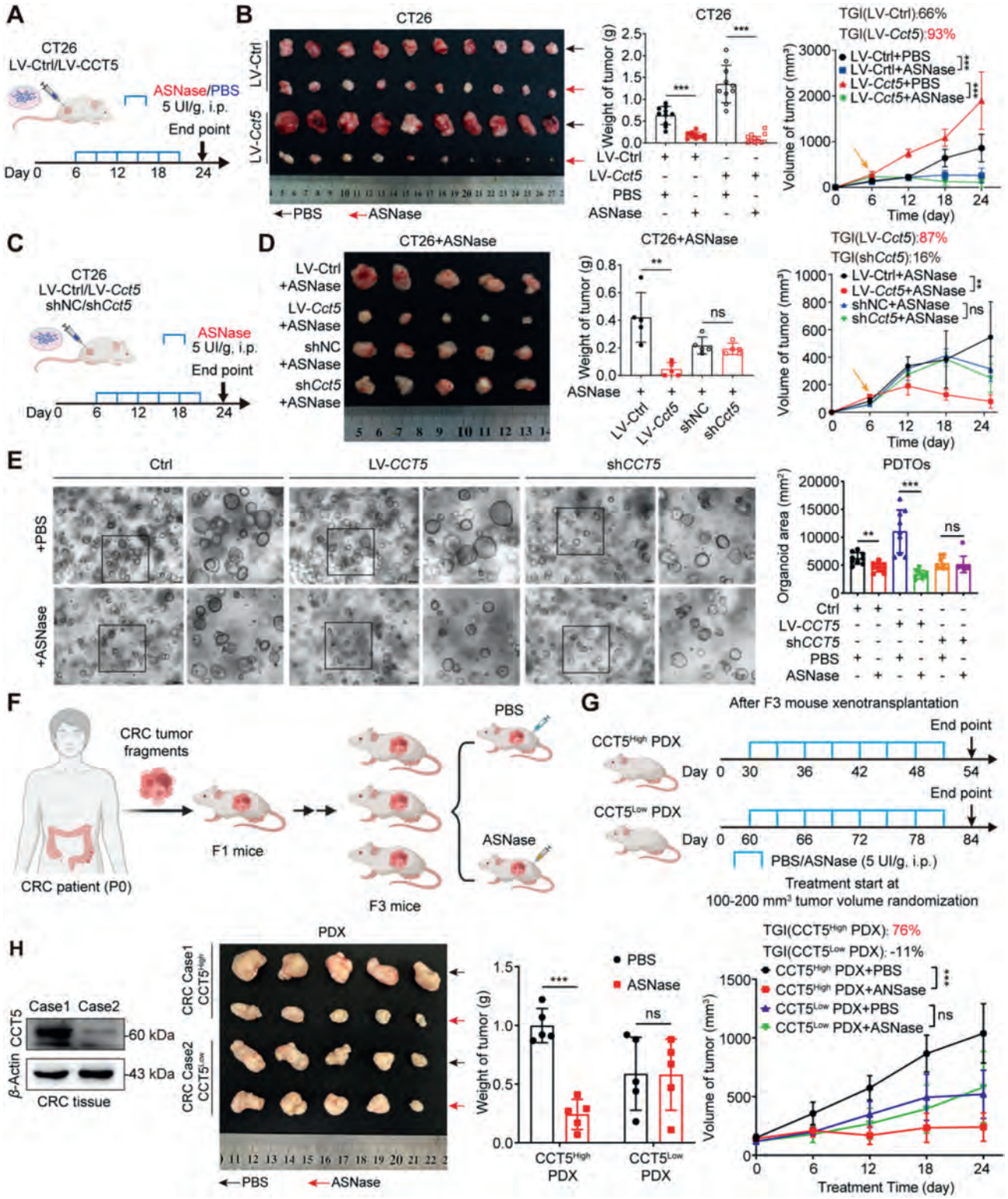

Figure 5 CCT5 as a biological marker to guide ASNase application for CRC growth inhibition. (A) The graph shows the protocol for ASNase or PBS treatment. (B) Representative images of subcutaneous tumors under the treatment of ASNase or PBS. The bar charts and line charts on the right quantified the weight and volume of subcutaneous tumors. The yellow arrow shows the start time of the treatment. $n = 10$. See also Supporting Information Fig. S9A and S9B. (C) The graph shows the treatment schedule for ASNase. (D) Representative images demonstrate the effect of ASNase on the growth of subcutaneous tumors. The bar charts and line charts on the right quantified the weight and volume of subcutaneous tumors. The yellow arrow shows the start time of the treatment. $n = 5$. See also Fig. S9C and S9D. (E) Representative images show the effect of ASNase on the growth of the *CCT5*-manipulated PDTOs. The scale bar = 100 μm. The statistical chart shows the average area of PDTOs under a 40× magnification field of view. $n = 3$. (F) Schematic diagram of PDX model construction. (G) Schematic of PBS/ASNase

tumor cells[29]. Western blot assays showed that after adding the mTORC1-specific inhibitor rapamycin (RAPA), the mTORC1 activated by overexpressed *CCT5* was restored, indicating that CCT5 specifically activated the mTORC1 pathway (Fig. 4C). Similarly, ASNase treatment reversed the activation of mTORC1 resulting from *CCT5* overexpression (Fig. 4D). Moreover, Asn supplementation restored mTORC1 inhibition due to *CCT5* knockdown (Fig. 4E). Administration of RAPA or ASNase resulted in significant growth inhibition of PDTOs overexpressing *CCT5* (Fig. 4F, G, I, and J). Furthermore, the growth inhibition induced by *CCT5* knockdown was reversed upon the addition of Asn (Fig. 4H and K). CRC cells also confirmed the mediating role of the Asn/mTORC1 axis in CCT5-stimulated proliferation (Fig. 4L–T). Notably, ASNase significantly inhibited the growth of PDTOs and CRC cells overexpressing *CCT5*, while no obvious inhibitory effect was observed in the control group (Fig. 4G). This finding suggests that CCT5 may serve as a specific biological marker for ASNase application.

3.5. CCT5 as a biological marker to guide ASNase application for CRC growth inhibition

As ASNase has been used in the clinical treatment of ALL, we further investigated its therapeutic potential in the CRC treatment by targeting the CCT5/Asn axis. We observed that ASNase reduced the size and weight of subcutaneous tumors formed by both control (LV-Ctrl) and *Cct5*-overexpressing (LV-*Cct5*) CRC cells compared to those treated with PBS. Subcutaneous tumors formed by LV-*Cct5* cells were more sensitive to ASNase treatment than those formed by LV-Ctrl cells (Fig. 5A and B). Consistently, the expression of *Cct5* was positively correlated with the expression of Ki67 and mTORC1 signaling pathway-related markers in subcutaneous tumors (Supporting Information Fig. S9A and S9B). Furthermore, we observed that ASNase treatment dramatically decreased the weight and size of subcutaneous tumors formed by LV-*Cct5* cells compared to those formed by LV-Ctrl cells, whereas it did not affect subcutaneous tumors formed by sh*Cct5* cells compared to those formed by shNC cells (Fig. 5C and D). There was no significant difference in the expression of Ki67 and mTORC1 signaling pathway-related markers in subcutaneous tumors formed by sh*Cct5* cells after treatment with ASNase (Fig. S9C and S9D). We further validated these findings using PDTOs models, and consistent results were obtained (Fig. 5E). To better preserve the genetic characteristics and heterogeneity of primary tumors, as well as to better predict the potential clinical efficacy of ASNase, we collected CRC tissues with high CCT5 expression and low CCT5 expression and constructed PDX models (Fig. 5F and G). We obtained the same results as before in the PDX models (Fig. 5H). These results strongly suggest a potential therapeutic role for ASNase in CCT5-overexpressing CRC tissues.

3.6. The Asn/mTORC1 axis mediates the effect of CCT5 on $CD8^+$ T cell function by upregulating the expression of PD-L1 in CRC cells

Several recent reports have demonstrated the regulatory relationship between amino acids and TME[25,30]. We observed a negative correlation between elevated expression of *CCT5* and immune pathways (Fig. 6A) as well as a negative correlation with the infiltration of $CD8^+$ T lymphocytes (Fig. 6B and Supporting Information Fig. S10A). The clinical analysis of CRC tissues showed that tumors with low CCT5 expression had 56% (10/18) of the CRC samples being CD3-positive and 67% (12/18) were CD8-positive (Fig. 6C). Subcutaneous tumors revealed greater infiltration of CD3- and CD8-positive cells in the control group compared to the group with *Cct5* overexpression (Fig. 6D).

We speculate whether CCT5 regulates $CD8^+$ T cells in the TME through Asn. *CCT5*-overexpressing CRC cells were co-cultured with peripheral blood mononuclear cells (PBMCs) isolated from healthy volunteers. As expected, a decrease in the proportion of $CD8^+$ and $CD69^+CD8^+$ T cells in PBMCs and a decrease in cytokine levels. Additionally, the effect of CCT5 on $CD8^+$ T cells was reversed by the addition of ASNase (Fig. 6E and Fig. S10B). However, the direct addition of Asn to PBMCs increased the quantity and activity of $CD8^+$ T cells, while the administration of ASNase could remove the effects caused by Asn (Fig. S10C and S10D). These findings suggest that CCT5-regulated effector $CD8^+$ T cell reduction is not directly triggered by Asn and may be driven by Asn-mediated changes in tumor cells.

GSEA was performed on the top 50 genes that were highly correlated with *CCT5* and revealed enrichment of PD-L1 expression and the PD-1 checkpoint pathway (Fig. 6F and Supporting Information Fig. S11A). Initially, co-culture experiments were performed using *CCT5*-overexpressing HCT116 cells and PBMCs. The results show that the proportion of $CD8^+PD\text{-}1^+$ cells did not change significantly (results not shown). However, *CCT5* overexpression was found to increase the expression of PD-L1, which was reversed by the administration of ASNase (Fig. 6G, I, and Fig. S11B). Moreover, the knockdown of *CCT5* reduced PD-L1 expression, while Asn supplementation restored the expression of PD-L1 (Fig. 6H and J, Fig. S11C). This result suggests that CCT5 regulates the expression of PD-L1 through Asn. Furthermore, to clarify whether the reduced $CD8^+$ T cell function caused by CCT5 overexpression is specifically triggered by the upregulation of PD-L1 expression, we added anti-PD-L1 antibody (atezolizumab, αPD-L1) treatment to the co-culture system. Results show that the suppression of $CD8^+$ T cell numbers and activity due to *CCT5* overexpression can be reversed after αPD-L1 treatment (Fig. 6K).

Previous research results have confirmed that Asn activates mTORC1 in CRC cells (Fig. 4A–E), and literature has reported that mTORC1 activation can upregulate the expression of PD-L1[31–34]. Based on this, we applied the mTORC1 inhibitor and found that administration of RAPA could reduce the upregulation of PD-L1 expression caused by CCT5 (Fig. 6L and M, Fig. S11D) and restore effector $CD8^+$ T cell numbers in PBMCs cocultured with *CCT5*-overexpressing HCT116 cells (Fig. 6N and Fig. S11E). Therefore, we propose that CCT5 upregulates the expression of PD-L1 in CRC cells through the Asn/mTORC1 axis, thereby reducing the function of $CD8^+$ T cells. Drug blockade at key links can effectively restore this negative effect (Fig. 6O). This provides us with a new idea for the treatment of CRC.

administration in PDX mice with high/low CCT5 expression. (H) Representative images show the effect of PBS/ASNase treatment on subcutaneous tumor growth in CCT5 high/low-expressing PDX mice. The bar charts and line charts on the right quantified the weight and volume of subcutaneous tumors. $n = 5$. Data are represented as mean ± SD. $^{**}P < 0.01$; $^{***}P < 0.001$; ns not significant.

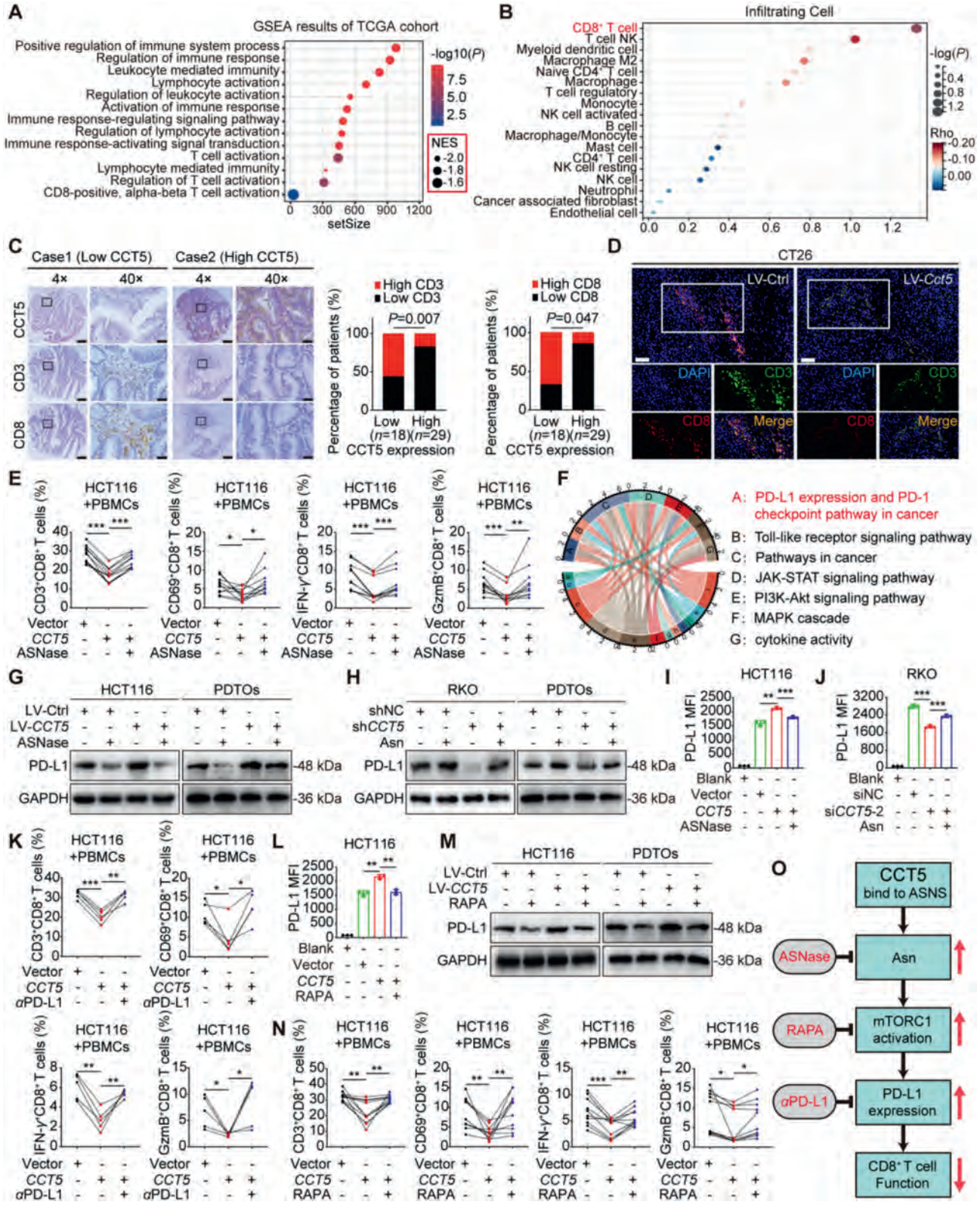

Figure 6 Asn-activated mTORC1 signaling upregulates PD-L1 expression to induce decreased $CD8^+$ T cell function. (A) *CCT5*-related pathways were enriched in CRC tissues using the TCGA database. (B) The correlation between *CCT5* expression and infiltrating immune cells in the CRC microenvironment was analyzed in the TIMER2.0 database (http://timer.comp-genomics.org/). See also Fig. S10A. (C) Representative IHC images show the expression of CCT5, CD3, and CD8 in CRC tissues. Scale bar = 500 μm in 4× figures and 50 μm in 40× figures. $n = 18$ (low CCT5) and 29 (high CCT5). (D) Representative multi-immunohistochemistry (mIHC) images demonstrate the expression of CD3 and CD8 in subcutaneous tumors. Scale bar = 60 μm. (E) FACS shows the effect of ASNase on the expression of indicated proteins or cytokines in PBMCs

3.7. Pharmacological values of targeting the CCT5/Asn/mTORC1/PD-L1 axis in CRC immunotherapy

Based on the positive regulation of PD-L1 expression by CCT5, we aimed to investigate whether CCT5 could serve as a molecular marker for predicting the efficacy of clinical anti-PD-L1 antibodies. We collected tumor tissues from six CRC patients who underwent αPD-L1 treatment. Among these patients, three exhibited a favorable response to the treatment, while the other three did not respond. IHC results indicated that, compared to the non-responsive group, the expression of CCT5 in the tumor epithelium of patients who responded to treatment was significantly elevated (Fig. 7A). These findings suggest that CCT5 expression in CRC patients is positively correlated with sensitivity to clinical αPD-L1 treatment. Further, we targeted the CCT5/Asn/mTORC1/PD-L1 axis to explore the potential of using ASNase and immune checkpoint inhibitors (ICIs) in combination therapy for CRC. In the co-culture system of CRC cells and PBMCs, we found that the combined application of ASNase and αPD-L1 seemed to be more effective compared to the individual treatment with either ASNase or αPD-L1, as indicated by the highest level of tumor cell apoptosis (Fig. 7B). Moreover, in the combination treatment group, the killing function of $CD8^+$ T cells was significantly restored, accompanied by a decrease in the expression of PD-L1 on tumor cells (Fig. 7C and D). The comparison revealed that the therapeutic effect of ASNase combined with αPD-L1 was the best in tumor cells of the *CCT5* overexpression group.

We further explored the value of *in vivo* combination therapy (Fig. 7E). ASNase and αPD-L1 combined therapy reduced the subcutaneous tumors formed by LV-*Cct5* and LV-Ctrl cells compared to those treated with PBS, ASNase, or αPD-L1 antibodies separately (Fig. 7F−H). Moreover, subcutaneous tumors formed by LV-*Cct5* cells were more sensitive to both ASNase monotherapy and combined ASNase and αPD-L1 therapy. However, no significant difference was observed in the subcutaneous tumors formed by sh*Cct5* cells among the various treatment groups. TGI analyses indicated that, among all the treatments conducted, the combined ASNase and αPD-L1 therapy exhibited the strongest tumor inhibition effect in subcutaneous tumors formed by LV-*Cct5* cells, with a TGI of up to 94% (Fig. 7I). The expression of proliferation index Ki67, mTORC1 signaling pathway-related markers, and PD-L1 was the lowest in subcutaneous tumors formed by LV-*Cct5* cells after ASNase and αPD-L1 combined therapy (Fig. 7J and Supporting Information Fig. S12A). Moreover, we collected mouse liver, lung, and spleen tissues after the combination treatment, and H&E staining showed that the combination therapy was not toxic (Fig. S12B). These results confirmed that combined treatment with ASNase and αPD-L1 antibodies can effectively inhibit CCT5-stimulated CRC proliferation.

4. Discussion

The molecular complexity of CRC contributes to its aberrant proliferation and suboptimal clinical response to therapies. In this study, we have provided the first evidence that CCT5 is associated with CRC progression. We found that CCT5 increases Asn biosynthesis by directly surrounding the unfolded asparagine synthetase *via* the apical domain and enhancing its enzymatic activity. On one hand, the augmented CCT5-mediated Asn synthesis activates the mTORC1 pathway in CRC cells, promoting CRC proliferation. On the other hand, mTORC1 activation upregulates the expression of PD-L1 in tumor cells, leading to a decrease in effector $CD8^+$ T cells in the TME, promoting immune escape of tumor cells, and further enhancing CRC proliferation. Importantly, we have demonstrated the efficacy of ASNase in CRC treatment, and the combination therapy of αPD-L1 antibodies effectively suppresses the proliferation of CCT5-high-expressing CRC (Fig. 8). These findings reveal CCT5 as a biological marker for assessing the response to targeted Asn metabolism combined with anti-PD-L1 immunotherapy in CRC.

The primary function of the chaperonin protein TRiC is to assist protein folding and contribute to the maintenance of cellular protein homeostasis. It is currently estimated that TRiC can fold approximately 10% of the newly synthesized proteins[35]. Elevated TRiC expression has also been demonstrated to be closely associated with abnormal proliferation of various tumor cells[36]. Here, we established for the first time the stimulatory role of one of its subunits, CCT5, in CRC proliferation. The ATP-binding equatorial domain (1−154 and 418−541 aa), the apical domain (227−380 aa) that binds to unfolded proteins, and the intermediate domain (155−226 and 381−417 aa) that undergoes nucleotide-induced conformational changes can be found in all the subunits of TRiC[37], and individual TRiC subunits also possess the ability to assist protein folding[38]. A major difference among various TRiC subunits exists in the apical domain, which might contribute to the unique recognition specificity of their interacting proteins[39]. In this study, ASNS was identified as a protein that specifically interacts with CCT5. Consistent with its binding properties to unfolded proteins, we confirmed direct binding between the CCT5 apical domain and the entire ASNS protein. Moreover, the interaction between CCT5 and ASNS did not alter the abundance of ASNS but induced a pronounced elevation in enzymatic activity, thereby facilitating the biosynthesis of Asn. Molecular chaperones maintain the active conformation of interacting proteins, and the CCT complex has been reported to stabilize the conformation of wild-type p53 to promote its activity[40]. Therefore, we speculated that the aberrantly high expression of CCT5 in conjunction with ASNS could stabilize the enzymatically active conformation of ASNS and stimulate the synthesis of Asn in CRC. This finding expands our understanding of TRiC's function as a molecular

co-cultured with control or *CCT5*-manipulated HCT116 cells. $n = 9$. See also Fig. S10B. (F) Pathway enrichment analysis of the top 50 *CCT5*-correlated genes in CRC chip data (GSE51254). See also Fig. S11A. (G−J) Western blot assays (G, H) and FACS analyses (I, J) demonstrate the expression of PD-L1 in *CCT5*-manipulated CRC cells and PDTOs with or without the treatment of ASNase (G and I) and Asn (H, J). $n = 3$. See also Fig. S11B and S11C. (K) PBMCs were co-cultured with control or *CCT5*-overexpressing HCT116 cells, and FACS analyses show the effect of anti-PD-L1 antibody (atezolizumab, αPD-L1) on the expression of the indicated proteins or cytokines. $n = 5$. (L, M) FACS analyses (L) and Western blot assays (M) indicate the expression of PD-L1 in *CCT5*-manipulated CRC cells, with or without the treatment of RAPA. $n = 3$. See also Fig. S11D. (N) PBMCs were co-cultured with control or *CCT5*-overexpressing HCT116 cells, and FACS analyses show the effect of RAPA on the expression of the indicated proteins or cytokines. $n = 10$. See also Fig. S11E. (O) The model diagram of the CCT5/Asn/mTORC1/PD-L1 axis. Data are represented as mean ± SD. $^{**}P < 0.01$; $^{***}P < 0.001$.

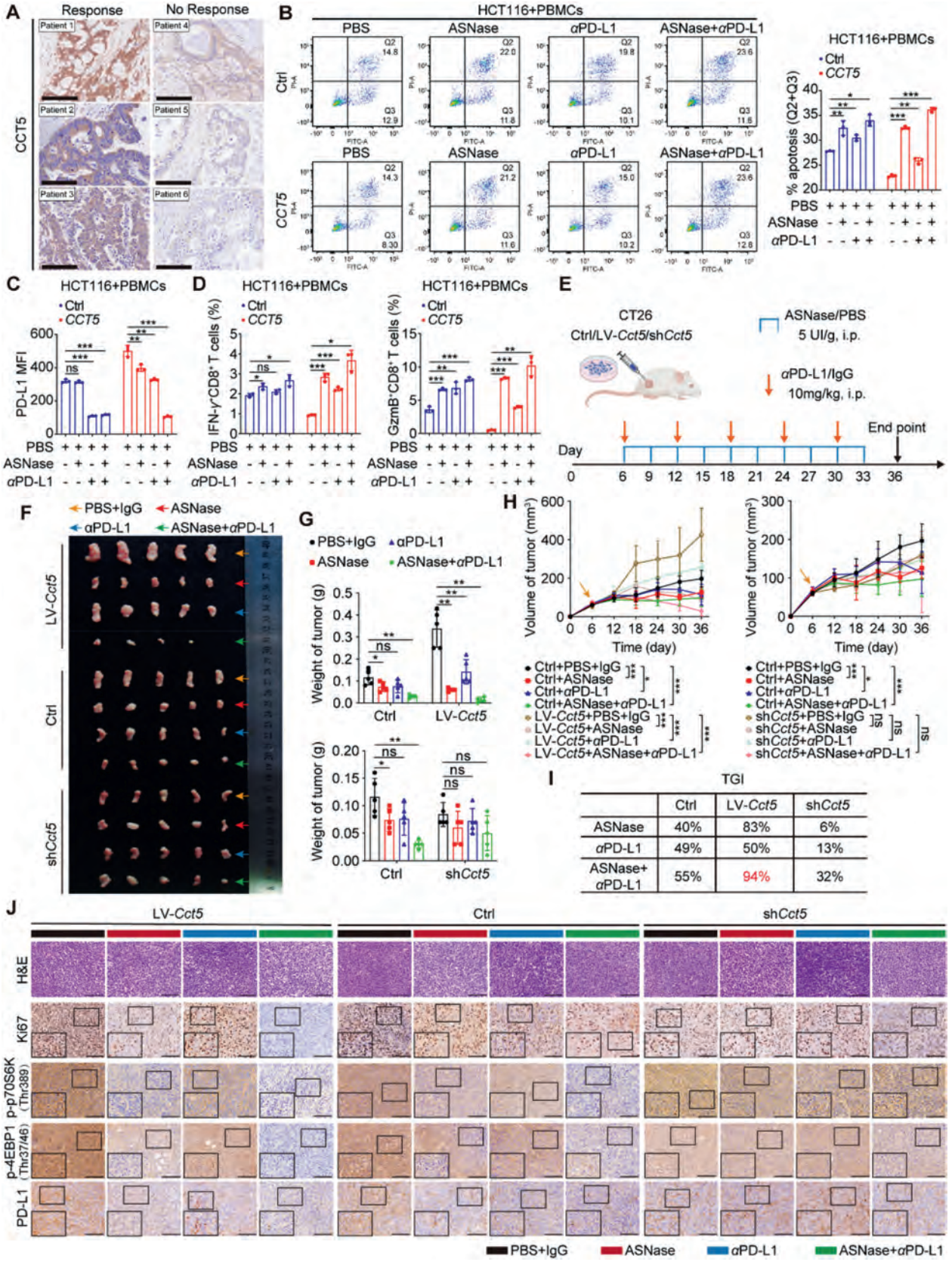

TGI	Ctrl	LV-*Cct5*	sh*Cct5*
ASNase	40%	83%	6%
αPD-L1	49%	50%	13%
ASNase+ αPD-L1	55%	94%	32%

Figure 7 Pharmacological values of targeting the CCT5/Asn/mTORC1/PD-L1 axis in CRC immunotherapy. (A) IHC staining of CCT5 in tissues from CRC patients receiving PD-L1 therapy. Scale bar = 100 μm. $n = 3$. (B) Apoptosis of tumor cells after co-culture of PBMCs with Ctrl or *CCT5*-overexpressing HCT116 cells. $n = 3$. (C) FACS results of PD-L1 expression in tumor cells after co-culture of PBMCs with Ctrl or *CCT5*-overexpressing HCT116 cells. $n = 3$. (D) Functional indices of $CD8^+$ T cells after co-culture of PBMCs with Ctrl or *CCT5*-overexpressing

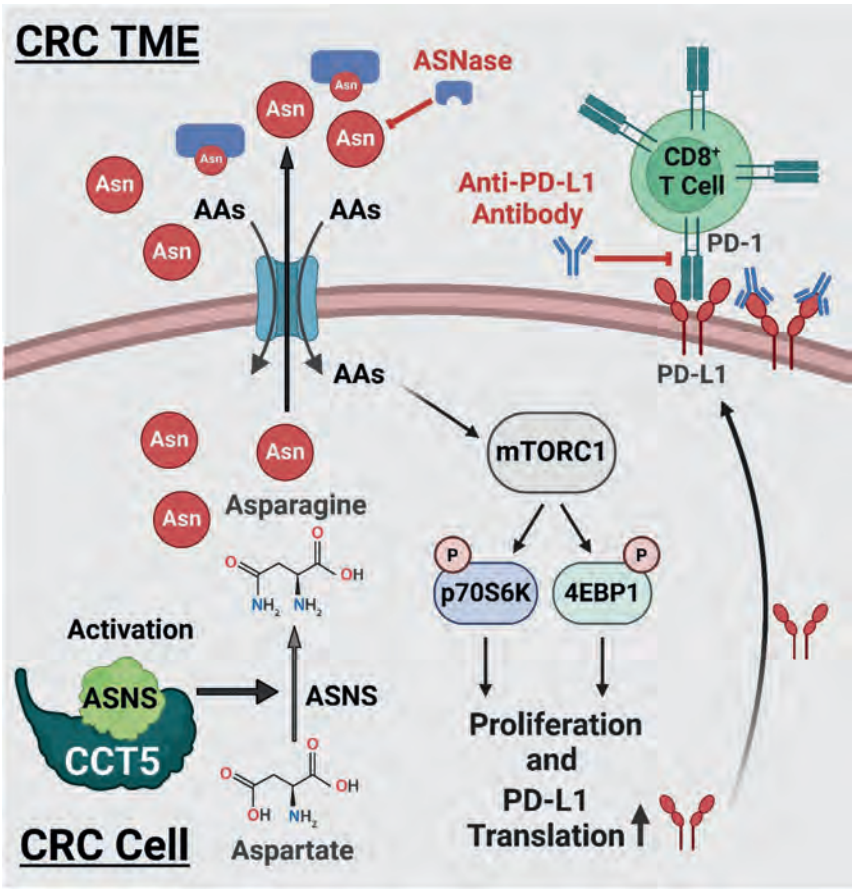

Figure 8 The Mechanism model of CCT5-mediated asparagine biosynthesis and anti-PD-L1 produces synergistic antitumor effects in colorectal cancer.

chaperone for protein homeostasis and provides the first evidence for its regulatory role in cellular amino acid metabolism. However, this finding was investigated only in CRC, and whether it is a universal phenomenon in normal colorectal mucosa or in other tumor cells remains to be explored.

Amino acids are essential building blocks of cells, and aberrant amino acid metabolism plays a crucial role in tumor progression, whereas depriving them can impede the aberrant growth of tumor cells[41]. The bioavailability of asparagine drives breast cancer metastasis and restores tumor cell death induced by glutamine depletion[42,43]. In this study, we demonstrated that CCT5 could stimulate the biosynthesis of Asn and promote the subsequent release of Asn into the extracellular space. The secreted Asn could potentially activate mTORC1 signaling to promote CRC cell proliferation by functioning as an amino acid exchange factor to facilitate the uptake of extracellular amino acids, such as serine, arginine, and histidine[29]. The impact of tumor amino acid metabolism on TME should not be overlooked. Here, we investigated the interaction between tumor and immune cells in the TME from the perspective of amino acid metabolism. We observed a significant decrease in effector $CD8^+$ T cells in CRC tissues with high CCT5 expression. Considering that high CCT5 expression is correlated with increased synthesis of Asn in tumors, we initially hypothesized that tumor-secreted Asn could directly inhibit the function of $CD8^+$ T cells in the TME. However, the administration of Asn directly to PBMCs *in vitro* could increase the quantity of $CD8^+$ T cells while simultaneously stimulating their function. This is consistent with an existing report that Asn can activate LCK signaling to enhance the anti-tumor response of $CD8^+$ T cells[44]. These phenomena contradicted our observations. As tumor

HCT116 cells. $n = 3$. (E) The treatment schedule for the monotherapy and combined therapy of ASNase and anti-PD-L1 antibody. (F) Representative images show the effect of ASNase and anti-PD-L1 monotherapy or combination therapy on the growth of subcutaneous tumors. $n = 5$. (G) The bar charts show the weight of subcutaneous tumors formed by *Cct5*-manipulated CT26 cells in BALB/c mice under the indicated treatments. $n = 5$. (H) The line charts illustrate the growth curve of subcutaneous tumors in BALB/c mice after the indicated treatments. The yellow arrow means the start time of the treatment. $n = 5$. (I) The table displays the TGI of BALB/c mice bearing subcutaneous tumors formed by *Cct5*-manipulated CT26 cells under the indicated treatments. (J) IHC staining shows the expression of Ki67, p-p70S6K, p-4EBP1, and PD-L1 in subcutaneous tumors. Scale bar = 100 μm. $n = 4$. See also Fig. S12A. Data are represented as mean ± SD (G, H). $^*P < 0.05$; $^{**}P < 0.01$; $^{***}P < 0.001$; ns not significant.

cells have a greater demand for nutrients than T cells[23], they may compete with T cells for Asn uptake in the TME to accomplish cell proliferation and survival. Considering the positive regulatory role of Asn in breast cancer cell metastasis[42], we speculate that tumor cells could prioritize the utilization of Asn to alter Asn levels in the TME, thereby manipulating T cells to evade immune surveillance[44].

PD-L1/PD-1 signaling is a key mechanism by which tumor cells inhibit T cell-mediated anti-tumor immune responses. Activation of this signaling axis inhibits T cell activation, proliferation, and cytotoxic secretion[45]. Specifically, upregulation of PD-L1 in tumor cells can bind to PD-1 on T cells, leading to dephosphorylation of CD3ζ and ZAP70 associated with the T cell receptor (TCR), and T cell activation is inhibited. This process inhibits the transmission of downstream signaling pathways (including PI3K/AKT and RAS/MEK/ERK pathways, etc.), thereby impairing T cell survival and proliferation. In addition, inhibition of PKCδ activation leads to reduced secretion of cytotoxic cytokines (such as IFN-γ) by T cells[46]. The expression of PD-L1 is regulated by multiple mechanisms. In addition to classical IFN-γ/JAK/STAT1 signaling, activation of the PI3K/AKT/mTOR oncogenic pathway promotes translation and expression of PD-L1 in various tumors such as gastric cancer, CRC, non-small cell lung cancer, and glioma[31−34]. It has been reported that mTORC1 activates downstream proteins such as 4E-BP1, STAT3, NF-κB, and c-MYC, which can upregulate the post-transcriptional translation of PD-L1[47]. Rapamycin inhibits mTORC1 and promotes autophagic degradation of PD-L1 protein[48]. In this study, we found that high expression of CCT5 in CRC upregulates the expression of PD-L1 in tumor cells and inhibits the cytotoxic function of $CD8^+$ T cells. The upregulation of PD-L1 may be mediated by Asn-activated mTORC1 signaling, as the expression of PD-L1 was restored upon supplementation with Asn in CCT5-silencing CRC cells. Moreover, either the addition of ASNase or treatment with the mTORC1 inhibitor RAPA resulted in decreased expression of PD-L1 and restoration of $CD8^+$ T cell function in CCT5-overexpressing CRC cells. Consequently, the overexpression of CCT5 in tumor cells results in enhanced synthesis of Asn, which may be preferentially utilized by tumor cells upon its secretion into the extracellular space.

Targeting PD-L1/PD-1 signaling has become the first-line therapy for multiple tumors. Similarly, targeting amino acid metabolism has been proven to have therapeutic benefits in various preclinical models[49]. Hence, combination therapy targeting both amino acid metabolism and ICIs may achieve durable antitumor effects and improve patient outcomes. Epacadostat, the indoleamine 2,3-dioxygenase 1 (IDO1) inhibitor, which affects tryptophan metabolism, was used in combination with PD-1 inhibitor Pembrolizumab in a further study on melanoma. In the initial non-randomized trials, the combined treatment showed hopeful efficacy without significant toxicity[50]. However, the therapeutic potential of targeting Asn to reverse the immune suppression in CRC needs to be further evaluated.

Therefore, we explored the therapeutic potential of ASNase-targeted Asn metabolism combined with immunotherapy in CRC. In this study, we demonstrated that ASNase alone has an inhibitory effect on CRC proliferation in BALB/c mice, with a TGI of approximately 40%−66%. Interestingly, in high CCT5-expressing CRC mice or PDX models, the application of ASNase resulted in a TGI of 76%−93%. We propose that this phenomenon occurs because ASNase reduces the elevated extracellular Asn levels resulting from CCT5 overexpression, thereby inhibiting the cancer-promoting Asn/mTORC1 signaling pathway. Simultaneously, it decreases the expression of PD-L1, which is upregulated by mTORC1 activation, thereby partially restoring the tumoricidal function of effector T cells.

In contrast, there was no significant difference in the inhibitory effect of ASNase on CRC when CCT5 was lowly expressed, indicating the potential guiding value of CCT5 expression in the application of ASNase treatment. Amino acid metabolism is a complex process, and CCT5 may not be the only regulator of Asn. After sh*CCT5*, the level of Asn may decrease in a short period, but during the long-term growth of tumor cells, there may be a compensatory pathway to re-promote Asn synthesis, offsetting the Asn level downregulated by sh*CCT5*, so that there was no significant difference in tumor volume compared with the Ctrl group treated with ASNase. Based on existing literature reports we speculate that, on the one hand, CCT5 as a molecular chaperone may cause misfolding or accumulation of proteins synthesized by cells after knockdown; on the other hand, the Asn level downregulated by sh*CCT5* may cause nutritional deficiency. These two effects may cause endoplasmic reticulum stress[51]. Under endoplasmic reticulum stress, the transcription factor ATF4 is upregulated, which can promote the transcriptional expression of ASNS and promote the biosynthesis of Asn[52]. This part of the mechanism needs to be further explored.

However, as shown in Fig. 6G and I, the use of ASNase could only restore the upregulation of PD-L1 expression mediated by CCT5 overexpression, but could not completely block the expression of PD-L1. In the TME, PD-L1 is expressed not only in tumor cells, but also in macrophages, dendritic cells, and B cells[46]. Therefore, some T cells are still suppressed, preventing them from fully restoring their ability to kill tumors. However, the use of anti-PD-L1 antibodies can completely block the activation of the PD-L1/PD-1 signaling pathway. Furthermore, we attempted to explore the therapeutic effect of anti-PD-L1 antibodies alone and in combination with ASNase in CRC with high expression of CCT5.

Through IHC experiments, we found that the expression of CCT5 in the epithelial tissue of CRC patients who clinically responded well to PD-L1 treatment was significantly higher than that of patients who did not respond to PD-L1 treatment. This suggests that the high expression of CCT5 may be positively correlated with PD-L1 treatment sensitivity in clinical CRC patients. However, there was no significant difference in the TGI between tumor-bearing mice injected with *Cct5*-overexpressing cells (50%) and those injected with control cells (49%) after anti-PD-L1 antibody treatment. But, tumor-bearing mice injected with *Cct5*-silencing cells showed a decrease in TGI (13%), indicating that high CCT5 expression is a sufficient but not necessary condition as a biomarker for anti-PD-L1 antibody treatment in CRC. Surprisingly, in mice under the combined treatment of ASNase and anti-PD-L1 antibodies, there was an improvement in TGI in the control, *Cct5*-overexpressing, and *Cct5*-knocked-down groups. More importantly, the inhibition rate in the subcutaneous tumors of mice with high *Cct5* expression reached 94%. Simultaneously, no significant organ damage was observed in mice after combination treatment.

Overall, the combination of ASNase and anti-PD-L1 therapy showed significant anti-tumor effects in CRC with high CCT5 expression. We hypothesize that, on one hand, ASNase suppresses aberrant tumor proliferation signals by inhibiting the CCT5/Asn/mTORC1 axis, while blocking CCT5-mediated sustained upregulation of PD-L1 expression in tumor cells. On the other hand, anti-PD-L1 antibodies block the activation of the PD-L1/PD-1 signaling axis between tumor cells, other cells in the TME, and T cells. This blockade reverses the immunosuppressive effects on T cells, enhances their tumor-killing capacity, and suppresses abnormal tumor growth.

Rapamycin has been approved by the FDA as an mTOR inhibitor, but we did not explore its effect in combination with anti-PD-L1 antibodies in this study. Because this study reported that Asn is located upstream of mTORC1 and has a positive activation effect on it, the removal of Asn by ANSase can also restore overactivated mTORC1 compared with the use of rapamycin. We believe that blocking the activation of the cancer signaling axis from a more upstream target may be more effective. Besides, the strategy of combining rapamycin or rapamycin analogs targeting mTOR with PD-L1 antibody therapy has been reported in many tumor studies[48,53]. It has also been reported that there are multiple feedback loops and compensatory pathways that promote cell survival and growth after rapamycin administration, making it impossible to completely block mTORC1-mediated signaling events[54]. However, as a first-line drug for childhood ALL, the therapeutic effect of ASNase in solid tumors still needs to be further explored, and its combination therapy with ICIs has not been reported, which is more valuable for research and provides new ideas for us to develop new and effective treatment strategies.

In existing clinical treatment guidelines, medication is often guided by the expression of certain biomarkers. For example, high expression of HER-2 promotes tumor progression in breast cancer. Trastuzumab (Herceptin) is effective in patients with HER-2-positive breast cancer but has no effect in patients with low HER-2 expression[55]. In summary, we have demonstrated the therapeutic potential of the combined treatment of ASNase and anti-PD-L1 antibodies in CRC and demonstrated that CCT5 could be used as a biomarker for combination treatment.

A limitation of the study is that the *in vivo* experiments were only done with subcutaneous tumor models, dismissing the role of the local tumor microenvironment of CRC, in particular the microbiome. We will further evaluate the effectiveness of ASNase combined with anti-PD-L1 antibody therapy in the orthotopic setting of CRC in follow-up studies.

5. Conclusions

This study discovered a new role for the chaperone protein CCT5 in amino acid metabolism and immune regulation. Mechanistically, CCT5 directly binds to ASNS to increase its activity and promote Asn biosynthesis. Tumor cells preferentially utilize the increased Asn synthesis, activate the mTORC1 signaling pathway, and promote tumor proliferation. At the same time, activated mTORC1 upregulates tumor cell PD-L1 expression, induces a decrease in the killing function of $CD8^+$ T cells in the TME, and ultimately leads to the malignant growth of CRC. In summary, we believe that CCT5 is a potential biomarker, which provides evidence for the application of combined therapy of ASNase and PD-L1 antibodies in CRC patients with high CCT5 expression.

Acknowledgments

Noncommunicable Chronic Diseases-National Science and Technology Major Project (2023ZD0500103, China), National Natural Science Foundation of China (82472895 and 82173172), Guangzhou Basic and Applied Basic Research Foundation (2024A04J6605, China) and China Postdoctoral Science Foundation (2022M721540 and 2023M741569, China).

Author contributions

Liang Zhao: Conceptualization, Supervision, Project administration, and Funding acquisition. Yujie Zhang: Conceptualization, Methodology, Investigation, Data Curation, Formal analysis, Writing - Original Draft, Writing - Review & Editing, Visualization. Weiyi Zhao: Investigation, Validation, Writing - Original Draft. Ling Wu: Formal analysis, Investigation, Writing - Review & Editing. Tianjing Ai: Validation, Investigation. Jie He: Validation. Zetao Chen: Methodology, Resources. Chuangyuan Wang: Software. Hui Wang: Funding acquisition. Rui Zhou: Funding acquisition. Chaoqun Liu: Funding acquisition.

Conflicts of interest

The authors declare no potential conflicts of interest.

Appendix A. Supporting information

Supporting information to this article can be found online at https://doi.org/10.1016/j.apsb.2025.03.026.

References

1. Bray F, Laversanne M, Sung H, Ferlay J, Siegel RL, Soerjomataram I, et al. Global cancer statistics 2022: GLOBOCAN estimates of incidence and mortality worldwide for 36 cancers in 185 countries. *CA Cancer J Clin* 2024;**74**:229−63.
2. Fan A, Wang B, Wang X, Nie Y, Fan D, Zhao X, et al. Immunotherapy in colorectal cancer: current achievements and future perspective. *Int J Biol Sci* 2021;**17**:3837−49.
3. Biller LH, Schrag D. Diagnosis and treatment of metastatic colorectal cancer: a review. *JAMA* 2021;**325**:669−85.
4. Whitesell L, Lindquist SL. HSP90 and the chaperoning of cancer. *Nat Rev Cancer* 2005;**5**:761−72.
5. Zhang Y, Wang Y, Wei Y, Wu J, Zhang P, Shen S, et al. Molecular chaperone CCT3 supports proper mitotic progression and cell proliferation in hepatocellular carcinoma cells. *Cancer Lett* 2016;**372**:101−9.
6. Tracz-Gaszewska Z, Klimczak M, Biecek P, Herok M, Kosinski M, Olszewski MB, et al. Molecular chaperones in the acquisition of cancer cell chemoresistance with mutated TP53 and MDM2 upregulation. *Oncotarget* 2017;**8**:82123−43.
7. Nardai G, Végh EM, Prohászka Z, Csermely P. Chaperone-related immune dysfunction: an emergent property of distorted chaperone networks. *Trends Immunol* 2006;**27**:74−9.
8. Alberti G, Vergilio G, Paladino L, Barone R, Cappello F, Conway de Macario E, et al. The chaperone system in breast cancer: roles and therapeutic prospects of the molecular chaperones Hsp27, Hsp60, Hsp70, and Hsp90. *Int J Mol Sci* 2022;**23**:7792.
9. Gracia B, Montes P, Gutierrez AM, Arun B, Karras GI. Protein-folding chaperones predict structure−function relationships and cancer risk in BRCA1 mutation carriers. *Cell Rep* 2024;**43**:113803.

10. Leitner A, Joachimiak LA, Bracher A, Mönkemeyer L, Walzthoeni T, Chen B, et al. The molecular architecture of the eukaryotic chaperonin TRiC/CCT. *Structure* 2012;**20**:814−25.
11. Li Y, Liu C, Zhang X, Huang X, Liang S, Xing F, et al. CCT5 induces epithelial-mesenchymal transition to promote gastric cancer lymph node metastasis by activating the Wnt/β-catenin signalling pathway. *Br J Cancer* 2022;**126**:1684−94.
12. Meng Y, Yang L, Wei X, Luo H, Hu Y, Tao X, et al. CCT5 interacts with cyclin D1 promoting lung adenocarcinoma cell migration and invasion. *Biochem Biophys Res Commun* 2021;**567**:222−9.
13. Vander Heiden MG, DeBerardinis RJ. Understanding the intersections between metabolism and cancer biology. *Cell* 2017;**168**:657−69.
14. Manna SK, Tanaka N, Krausz KW, Haznadar M, Xue X, Matsubara T, et al. Biomarkers of coordinate metabolic reprogramming in colorectal tumors in mice and humans. *Gastroenterology* 2014;**146**:1313−24.
15. Lieu EL, Nguyen T, Rhyne S, Kim J. Amino acids in cancer. *Exp Mol Med* 2020;**52**:15−30.
16. Cheng L, Wang X, Liu A, Zhu Y, Cheng H, Yu J, et al. Phenylalanine deprivation inhibits multiple myeloma progression by perturbing endoplasmic reticulum homeostasis. *Acta Pharm Sin B* 2024;**14**: 3493−512.
17. Deng L, Yao P, Li L, Ji F, Zhao S, Xu C, et al. p53-mediated control of aspartate-asparagine homeostasis dictates LKB1 activity and modulates cell survival. *Nat Commun* 2020;**11**:1755.
18. Du F, Chen J, Liu H, Cai YF, Cao TY, Han WL, et al. SOX12 promotes colorectal cancer cell proliferation and metastasis by regulating asparagine synthesis. *Cell Death Dis* 2019;**10**:239.
19. Richards NGJ, Kilberg MS. Asparagine synthetase chemotherapy. *Annu Rev Biochem* 2006;**75**:629−54.
20. Bader JE, Voss K, Rathmell JC. Targeting metabolism to improve the tumor microenvironment for cancer immunotherapy. *Mol Cell* 2020; **78**:1019−33.
21. Sun L, Suo C, Li ST, Zhang H, Gao P. Metabolic reprogramming for cancer cells and their microenvironment: beyond the Warburg effect. *Biochim Biophys Acta Rev Cancer* 2018;**1870**:51−66.
22. Shi D, Wu X, Jian Y, Wang J, Huang C, Mo S, et al. USP14 promotes tryptophan metabolism and immune suppression by stabilizing IDO1 in colorectal cancer. *Nat Commun* 2022;**13**:5644.
23. Chang CH, Qiu J, O'Sullivan D, Buck MD, Noguchi T, Curtis JD, et al. Metabolic competition in the tumor microenvironment is a driver of cancer progression. *Cell* 2015;**162**:1229−41.
24. Yang L, Chu Z, Liu M, Zou Q, Li J, Liu Q, et al. Amino acid metabolism in immune cells: essential regulators of the effector functions, and promising opportunities to enhance cancer immunotherapy. *J Hematol Oncol* 2023;**16**:59.
25. Han C, Ge M, Ho PC, Zhang L. Fueling T-cell antitumor immunity: amino acid metabolism revisited. *Cancer Immunol Res* 2021;**9**: 1373−82.
26. Schmitt M, Ceteci F, Gupta J, Pesic M, Böttger TW, Nicolas AM, et al. Colon tumour cell death causes mTOR dependence by paracrine P2X4 stimulation. *Nature* 2022;**612**:347−53.
27. Liu C, Pan Z, Chen Q, Chen Z, Liu W, Wu L, et al. Pharmacological targeting PTK6 inhibits the JAK2/STAT3 sustained stemness and reverses chemoresistance of colorectal cancer. *J Exp Clin Cancer Res* 2021;**40**:297.
28. Gestaut D, Zhao Y, Park J, Ma B, Leitner A, Collier M, et al. Structural visualization of the tubulin folding pathway directed by human chaperonin TRiC/CCT. *Cell* 2022;**185**:4770−87.e20.
29. Krall AS, Xu S, Graeber TG, Braas D, Christofk HR. Asparagine promotes cancer cell proliferation through use as an amino acid exchange factor. *Nat Commun* 2016;**7**:11457.
30. Huang H, Vandekeere S, Kalucka J, Bierhansl L, Zecchin A, Brüning U, et al. Role of glutamine and interlinked asparagine metabolism in vessel formation. *EMBO J* 2017;**36**:2334−52.
31. Koh V, Chakrabarti J, Torvund M, Steele N, Hawkins JA, Ito Y, et al. Hedgehog transcriptional effector GLI mediates mTOR-Induced PD-L1 expression in gastric cancer organoids. *Cancer Lett* 2021;**518**: 59−71.
32. Huang TY, Chang TC, Chin YT, Pan YS, Chang WJ, Liu FC, et al. NDAT targets PI3K-mediated PD-L1 upregulation to reduce proliferation in gefitinib-resistant colorectal cancer. *Cells* 2020;**9**: 1830.
33. Lastwika KJ, Wilson W, Li QK, Norris J, Xu H, Ghazarian SR, et al. Control of PD-L1 expression by oncogenic activation of the AKT−mTOR pathway in non-small cell lung cancer. *Cancer Res* 2016;**76**:227−38.
34. Parsa AT, Waldron JS, Panner A, Crane CA, Parney IF, Barry JJ, et al. Loss of tumor suppressor PTEN function increases B7-H1 expression and immunoresistance in glioma. *Nat Med* 2007;**13**:84−8.
35. Yam AY, Xia Y, Lin HTJ, Burlingame A, Gerstein M, Frydman J. Defining the TRiC/CCT interactome links chaperonin function to stabilization of newly made proteins with complex topologies. *Nat Struct Mol Biol* 2008;**15**:1255−62.
36. Ghozlan H, Showalter A, Lee E, Zhu X, Khaled AR. Chaperonin-containing TCP1 complex (CCT) promotes breast cancer growth through correlations with key cell cycle regulators. *Front Oncol* 2021; **11**:663877.
37. Lopez T, Dalton K, Frydman J. The mechanism and function of group II chaperonins. *J Mol Biol* 2015;**427**:2919−30.
38. Sergeeva OA, Chen B, Haase-Pettingell C, Ludtke SJ, Chiu W, King JA. Human CCT4 and CCT5 chaperonin subunits expressed in Escherichia coli form biologically active homo-oligomers. *J Biol Chem* 2013;**288**:17734−44.
39. Balchin D, Miličić G, Strauss M, Hayer-Hartl M, Hartl FU. Pathway of actin folding directed by the eukaryotic chaperonin TRiC. *Cell* 2018;**174**:1507−21.e16.
40. Trinidad AG, Muller PAJ, Cuellar J, Klejnot M, Nobis M, Valpuesta JM, et al. Interaction of p53 with the CCT complex promotes protein folding and wild-type p53 activity. *Mol Cell* 2013;**50**: 805−17.
41. Pokrovsky VS, Chepikova OE, Davydov DZ, Zamyatnin AA, Lukashev AN, Lukasheva EV. Amino acid degrading enzymes and their application in cancer therapy. *Curr Med Chem* 2019;**26**: 446−64.
42. Knott SRV, Wagenblast E, Khan S, Kim SY, Soto M, Wagner M, et al. Asparagine bioavailability governs metastasis in a model of breast cancer. *Nature* 2018;**554**:378−81.
43. Luo M, Brooks M, Wicha MS. Asparagine and glutamine: co-conspirators fueling metastasis. *Cell Metab* 2018;**27**:947−9.
44. Wu J, Li G, Li L, Li D, Dong Z, Jiang P. Asparagine enhances LCK signalling to potentiate $CD8^+$ T-cell activation and anti-tumour responses. *Nat Cell Biol* 2021;**23**:75−86.
45. Han Y, Liu D, Li L. PD-1/PD-L1 pathway: current researches in cancer. *Am J Cancer Res* 2020;**10**:727−42.
46. Wu M, Huang Q, Xie Y, Wu X, Ma H, Zhang Y, et al. Improvement of the anticancer efficacy of PD-1/PD-L1 blockade via combination therapy and PD-L1 regulation. *J Hematol Oncol* 2022; **15**:24.
47. Quan Z, Yang Y, Zheng H, Zhan Y, Luo J, Ning Y, et al. Clinical implications of the interaction between PD-1/PD-L1 and PI3K/AKT/mTOR pathway in progression and treatment of non-small cell lung cancer. *J Cancer* 2022;**13**:3434−43.
48. Yu J, Ling S, Hong J, Zhang L, Zhou W, Yin L, et al. TP53/mTORC1-mediated bidirectional regulation of PD-L1 modulates immune evasion in hepatocellular carcinoma. *J Immunother Cancer* 2023;**11**: e007479.
49. Lukey MJ, Katt WP, Cerione RA. Targeting amino acid metabolism for cancer therapy. *Drug Discov Today* 2017;**22**:796−804.
50. Long GV, Dummer R, Hamid O, Gajewski TF, Caglevic C, Dalle S, et al. Epacadostat plus pembrolizumab *versus* placebo plus pembrolizumab in patients with unresectable or metastatic melanoma (ECHO-301/KEYNOTE-252): a phase 3, randomised, double-blind study. *Lancet Oncol* 2019;**20**:1083−97.

51. Chen X, Shi C, He M, Xiong S, Xia X. Endoplasmic reticulum stress: molecular mechanism and therapeutic targets. *Sig Transduct Target Ther* 2023;**8**:1−40.
52. Siu F, Bain PJ, LeBlanc-Chaffin R, Chen H, Kilberg MS. ATF4 is a mediator of the nutrient-sensing response pathway that activates the human asparagine synthetase gene. *J Biol Chem* 2002;**277**: 24120−7.
53. Enhanced bypass of PD-L1 translation reduces the therapeutic response to mTOR kinase inhibitors. *Cell Rep* 2023;**42**:112764.
54. Li J, Kim SG, Blenis J. Rapamycin: one drug, many effects. *Cell Metab* 2014;**19**:373−9.
55. Slamon D, Eiermann W, Robert N, Pienkowski T, Martin M, Press M, et al. Adjuvant trastuzumab in HER2-positive breast cancer. *N Engl J Med* 2011;**365**:1273−83.